Distributed Source–Load–Storage Cooperative Low-carbon Scheduling Strategy Considering Vehicle-to-grid Aggregators

Xiao Xu, Ziwen Qiu, Teng Zhang, and Hui Gao

***Abstract*—The vehicle-to-grid (V2G) technology enables the bidirectional power flow between electric vehicle (EV) batteries and the power grid, making EV-based mobile energy storage an appealing supplement to stationary energy storage systems. However, the stochastic and volatile charging behaviors pose a challenge for EV fleets to engage directly in multi-agent cooperation. To unlock the scheduling potential of EVs, this paper proposes a source–load–storage cooperative low-carbon scheduling strategy considering V2G aggregators. The uncertainty of EV charging patterns is managed through a rolling-horizon control framework, where the scheduling and control horizons are adaptively adjusted according to the availability periods of EVs. Moreover, a Minkowski-sum based aggregation method is employed to evaluate the scheduling potential of aggregated EV fleets within a given scheduling horizon. This method effectively reduces the variable dimension while preserving the charging and discharging constraints of individual EVs. Subsequently, a Nash bargaining based cooperative scheduling model involving a distribution system operator (DSO), an EV aggregator (EVA), and a load aggregator (LA) is established to maximize the social welfare and improve the low-carbon performance of the system. This model is solved by the alternating direction method of multipliers (ADMM) algorithm in a distributed manner, with privacy of participants fully preserved. The proposed strategy is proven to achieve the objective of low-carbon economic operation.**

***Index Terms*—Electric vehicle (EV), low-carbon scheduling, mobile storage system, Nash bargaining, power flexibility, alternating direction method of multipliers (ADMM).**

I. Introduction

ELECTRIFICATION of mobility provides a promising solution to decarbonizing the transportation sector by enabling zero-emission transportation. With the mass adoption of electric vehicles (EVs), the worldwide deployment of EVs doubled in 2021 compared with 2020, reaching a new record of 6.6 million [1]. As EVs are powered by onboard battery packs that get charged at dedicated charging stations (CSs), the stochastic travelling patterns and the consequent uncertain charging behaviors of widely deployed EVs can result in grid congestion, increased energy losses, and aggravated peak-to-valley difference [2]. Meanwhile, owing to the vehicle-to-grid (V2G) technology, the standby EVs can operate as schedulable storage systems, making them ideal complementary resources to stationary energy storage systems. By coordinating with stationary energy storages and renewables, improved peak shaving, enhanced renewable hosting, and cooperative carbon reduction can be expected [3].

Although the coordinated scheduling of EVs and distributed generations (DGs) is beneficial to the modern power systems, their uncertainty issue, aggregation method, and cooperative strategy pose challenges in decision-making. As a result, existing research can be divided into three main categories.

The first category is on the uncertainty associated with EVs. The uncertainty in the operation states of DGs like solar photovoltaics (PVs) and wind turbines can be addressed by adequately modelling their environmental dependence [4]-[6]. In contrast, EV charging behavior exhibits significant randomness and is influenced by factors such as battery state of charge (SoC), charging price, traffic condition, travel patterns of users, and charging mode selection [7]. While numerous forecasting methods have been proposed in the existing literature on EV charging behavior simulation, the majority are grounded in statistic modelling [8] or the Markov decision-making process [9], with only partial consideration given to the aforementioned factors. Furthermore, these forecasting methods are typically used to investigate the grid impacts of large-scale EV charging, with little insight into the charging scheduling of an EV fleet under uncertainty. Instead of relying on forecasting methods, some studies [10], [11] inquire users about their charging plans before arrival. However, this kind of method raises concerns about potential privacy violations and questions about whether users can provide accurate travel and charging plans.

The second category is on the aggregation method of EVs. An effective aggregation method enables geographically dispersed EVs to enter the electricity market as a unified entity, namely, an EV aggregator (EVA) [12]. As the interme-

Manuscript received: October 1, 2023; revised: January 11, 2024; accepted: February 8, 2024. Date of CrossCheck: February 8, 2024. Date of online publication: March 30, 2024.

This work was partially supported by the National Natural Science Foundation of China (General Program) (No. 52077107) and Natural Science Research Start-up Foundation of Recruiting Talents of Nanjing University of Posts and Telecommunications (No. NY220082).

X. Xu (corresponding author), Z. Qiu, T. Zhang, and H. Gao are with the School of Automation, Nanjing University of Posts and Telecommunications, Nanjing, 210023, China (e-mail: xu.xiao@njupt.edu.cn; ziwen_qiu@sina.com; teng_zhang_sg@sina.com; gaoh@njupt.edu.cn).

DOI: 10.35833/MPCE.2023.000742

diary between the distribution system operator (DSO) and EVs, EVA pursues the most profitable charging and discharging schemes while minimizing disruption to charging needs of users. To achieve this, it is critical for EVA to precisely evaluate the scheduling potential of EV fleets over time. The existing literature [13]-[15] predominantly employs the individual modelling approach in the EV aggregation, representing EVA by the sum of all individual EV models. However, incorporating all of those individual EV models into the scheduling model could introduce an excessive number of new variables and constraints, potentially leading to scalability issues with large-scale EV fleets. For example, the day-ahead power regulation capability of EVA is evaluated in [13] and [14] based on forecasting the charging patterns of individual EVs. The scheduling potential of EVA is estimated based on the preferred charging strategies inquired from EV users in [15].

The third category is on the cooperation and energy trading strategies between EVA and other agents, which is commonly based on game theory. The game theory enables agents with inconsistent decision-making strategies to coordinate benefits, thereby facilitating the cooperation and energy trading among multiple agents [16]. A Nash bargaining based cooperative approach is proposed in [17] for the coordinated scheduling of EVs and integrated energy systems (IESs), aiming at minimizing the operating costs for both agents. However, it assumes that the charging plans of EVs can be precisely forecasted one day in advance. A day-ahead and intraday charging scheduling model is proposed in [18] for multiple EVAs, where the cooperative charging scheduling is established based on the generalized Nash bargaining. Similarly, a Nash bargaining based price bidding strategy is proposed in [19] for the competition among EVAs, aiming at compensating the supply and demand imbalance. However, the charging scheduling models in [18] and [19] are solved in a centralized manner without considering the privacy concerns. To preserve the privacy of EV users, [20] proposes a neurodynamic-based approach to solve the charging scheduling model of EVAs in a distributed manner. Other related works [21], [22] employ leader-follower games (e.g., Stackelberg game) to simulate the energy trading process between EVA and other agents. All the studies above aim at achieving either joint profit maximization or cost minimization, with minimal consideration given to potential for coordinated carbon reduction. Additionally, the power flexibility of EVA is computed under the assumption that the charging patterns of EV users can be anticipated through forecasting or inquiry.

To summarize, previous research has offered ample models and theoretical background for the cooperative scheduling problem of EVA and other agents. Nonetheless, there are still some research gaps in this field.

1) The uncertainty issue associated with EV charging patterns is not fully addressed on EV charging scheduling. While methods such as random sampling and Markov decision-making process have been employed to forecast EV status, they are typically dependent on predefined probability distributions of charging parameters that are only suitable for large-scale EV fleets with consistent charging patterns.

2) The aggregation method of EVs is dominant with the individual modelling approach, where each EV has its own schedulable power region modelled individually. Then, all individual EV models are summed to compute the power flexibility of EVA. Nevertheless, the associated constrained aggregation process can be computationally intensive and may confront scalability issues, particularly when dealing with a large number of EVs.

3) Current research on the coordination strategies between EVA and other agents has primarily concentrated on profit maximization or cost minimization while dedicating less effort to exploring the potential for coordinated carbon reduction. Additionally, the influence of uncertain EV charging behaviors and the aggregation method on the practicability of the coordination strategies have not been thoroughly examined.

Given the aforementioned research gaps, this paper proposes a distributed source−load−storage cooperative low-carbon scheduling strategy considering V2G aggregators. Firstly, a rolling-horizon control framework is presented to address the uncertainty related to EV charging behaviors. Secondly, a Minkowski-sum based aggregation method is proposed to evaluate the scheduling potential of EVA within the scheduling horizon. Finally, a cooperative game model is developed for the coordinated operation of DSO, EVA, and load aggregator (LA), along with a distributed solving algorithm. Correspondingly, the main contributions of this paper are summarized as follows.

1) Using a rolling-horizon control framework enables the update of input parameters in the scheduling model to react to any deviations from the previous state. The uncertainty associated with EV charging behaviors can be managed by adapting the scheduling and control horizons according to the availability periods of EVs.

2) The Minkowski-sum based aggregation method aims to reduce the number of variables and constraints fed to the scheduling model while preserving the scheduling constraints of individual EVs. When incorporated into the rolling-horizon control framework, this method allows for a dynamic assessment on the scheduling potential of EVA.

3) The cooperative low-carbon scheduling strategy can be implemented in real time with the rolling-horizon control framework and flexible aggregation method. The cooperative scheduling model, with integrated electricity and carbon trading, maximizes the profits of all involved agents while improving the low-carbon performance of the entire system. Furthermore, this model is solved in a distributed manner using the alternating direction method of multipliers (ADMM) algorithm to preserve privacy during the interactions among DSO, LA, and EVA.

The rest of this paper is organized as follows. Section II introduces the cooperative scheduling with rolling-horizon control framework. Section III provides the evaluation on scheduling potential for EVA. Section IV presents the decision-making models for each agent. Section V introduces the source−load−storage cooperative low-carbon scheduling model and its distributed solving algorithm. Sections VI and VII

give the case study and conclusions, respectively.

II. Cooperative Scheduling with Rolling-horizon Control Framework

This section introduces a rolling-horizon control framework to manage the uncertainty in EV charging patterns. Following this, a cooperative scheduling strategy of DSO, EVA, and LA is proposed to achieve optimal real-time scheduling solutions.

A. Rolling-horizon Control Framework

The proposed cooperative scheduling aims to maximize the profits of DSO, EVA, and LA jointly while pursuing collaborative carbon reduction via electricity and carbon trading. To achieve this, the three agents actively regulate their schedulable devices from both the source and load sides. The source-side schedulable devices for the system under test encompass the gas turbine generators (GTGs) and renewable systems, while the load-side schedulable devices incorporate transferable flexible loads. The V2G-supported EVs act as distributed battery storage systems, and their appropriate charging and discharging scheduling assist in managing fluctuations in both supply and demand. The interaction framework of multi-agent system under test is shown in Fig. 1. In particular, DSO seeks to minimize its operating costs by actively scheduling the power exchange with LAs and EVAs under the constraint of the supply-demand balance. LAs aim to maximize their revenues via the price-based demand response, while EVAs aim to increase their revenues from V2G service and price incentives driven by reduced carbon emissions.

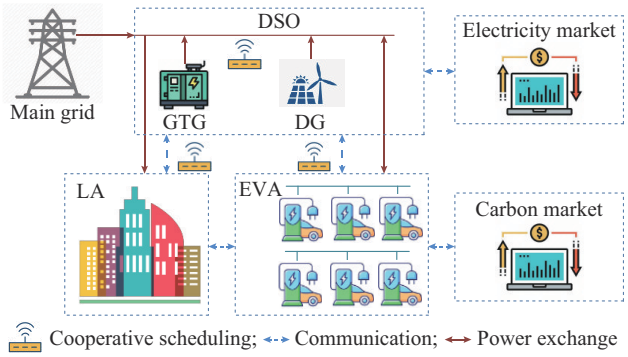

Fig. 1. Interaction framework of multi-agent system.

To address the impact of uncertain EV charging patterns on the feasibility of charging scheduling, the cooperative scheduling of DSO, EVA, and LA is implemented using a rolling-horizon control framework, as illustrated in Fig. 2. The basic idea of the rolling-horizon control is to evaluate the scheduling potential of agents in the scheduling horizon on the basis of the current states of the schedulable devices, solve the cooperative scheduling model, and implement the optimal decision-making results in the control horizon. For a given scheduling horizon, it is divided into several equal-size intervals. The optimal decision-making solution can be determined for the entire scheduling horizon. In each rolling scheduling horizon, the first interval allocated for implementing control actions is referred to as the control horizon, while the remaining time intervals are utilized for initializing the next scheduling horizon.

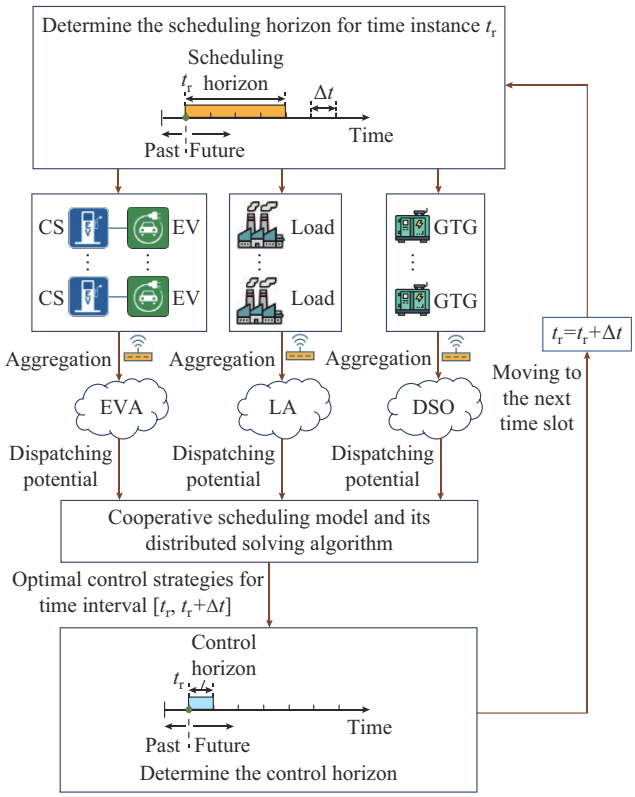

Fig. 2. Rolling-horizon control framework for cooperative scheduling of DSO, EVA, and LA.

B. Rolling-horizon Scheduling of EVA

Rolling-horizon control is a well-established technique for tackling real-time/online control challenges in the presence of uncertainty. It has been extensively applied in the scheduling of DGs [23] and flexible loads [24]. As depicted in Fig. 2, the rolling-horizon control involves a scheduling horizon and a control horizon. The scheduling horizon is the time frame within which all related uncertain parameters are assumed to be known with some degree of certainty. The control horizon refers to the time frame within which the optimal decision variables for the scheduling horizon are implemented. By moving the two horizons forward and solving the decision-making model through rolling-horizon optimization (RHO), the uncertainty parameters can be incorporated into the scheduling process. The length of the scheduling horizon for DGs or flexible loads is typically fixed and determined by either the time frame capable of reliably predicting power output or the contracted flexible period. In contrast, EVs are characterized by heterogenous charging behaviors, and the resulting stochastic availability periods suggest that the length of scheduling horizon must be adaptively adjusted.

Considering uncertain parameters like the external variability in EV charging requests and the wholesale electricity price, the rolling-horizon control framework for the charging scheduling of EV fleets can be defined by the following steps, as shown in Fig. 3.

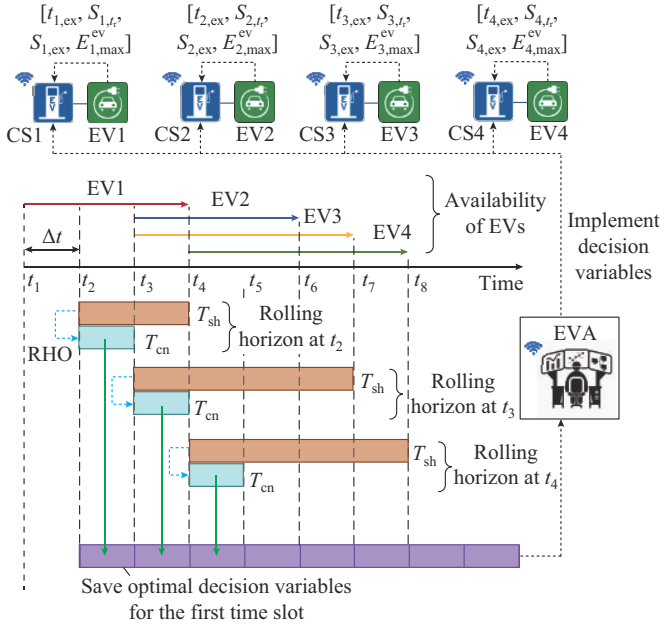

Fig. 3. Determination of scheduling and control horizons for EVA in a rolling approach.

1) The time axis is partitioned into a sequence of equal-size intervals, with the length of each interval equaling Δt.

2) At a real-time instance t_r, each CS transmits the charging information of the EV connected to EVA via established communication interfaces. The charging information includes the expected departure time, the current battery SoC, the expected departure SoC, and the rated battery capacity. Utilizing this data, the charging scheduling feasibility of each EV can be evaluated using (1). If (1) is satisfied, the availability period of the EV connected to CS can be determined as (2). Otherwise, the EV has to be charged or discharged at the full power of the CS during the remaining charging periods without any scheduling flexibility. Afterwards, the scheduling horizon of EVA can be computed as the union of all individual availability periods, as in (3).

$$\begin{cases} t_r+(S_{i,ex}-S_{i,tr})E^{ev}_{i,max}/P^{ev,c}_{i,max}<t_{i,ex} & S_{i,ex}>S_{i,tr} \\ t_r+(S_{i,tr}-S_{i,ex})E^{ev}_{i,max}/P^{ev,d}_{i,max}<t_{i,ex} & S_{i,ex}\le S_{i,tr} \end{cases} \tag{1}$$

$$T_{i,a}=[t_r, t_{i,ex}] \tag{2}$$

$$T_{sh}=\bigcup T_{i,a} \quad i\in N^{ev}_{tr} \tag{3}$$

where $t_{i,ex}$ and $S_{i,ex}$ are the expected departure time and battery SoC of the i^{th} EV that is currently being charged, respectively; $S_{i,tr}$ is the battery SoC of the i^{th} EV at time t_r, with the rated battery capacity represented by $E^{ev}_{i,max}$; $T_{i,a}$ is the availability period of the i^{th} EV; T_{sh} and N^{ev}_{tr} are the scheduling horizon and the number of EVs available for charging scheduling at time t_r, respectively; and $P^{ev,c}_{i,max}$ and $P^{ev,d}_{i,max}$ are the maximum charging and discharging power of the CS connected by the i^{th} EV , respectively.

3) Based on the collected charging information and the availability periods of EVs being charged within the scheduling horizon T_{sh}, EVA conducts RHO in accordance with its decision-making model. The first time slot of T_{sh} is considered as the control horizon T_{cn}, within which its optimal decision variables will be executed in the CS for charging scheduling.

4) Move forward to the next time instance ($t_r+\Delta t$) and update the uncertain parameters.

5) Repeat the steps above until the last scheduling period is reached, as illustrated in Fig. 3.

C. Cooperative Scheduling of DSO, EVA, and LA

With the uncertainty of EV charging incorporated, the generalized implementation procedure of the cooperative scheduling of DSO, EVA, and LA is summarized as follows.

1) First, at real-time instance t_r, the scheduling horizon for each agent can be determined based on the availability periods of the online schedulable devices for an agent. The scheduling horizon of all three agents can be determined by finding the intersection of their individual scheduling horizons to ensure a consistent scheduling time frame, as in (4).

$$T_{sh}=T^{DSO}_{sh}\bigcap T^{EVA}_{sh}\bigcap T^{LA}_{sh} \tag{4}$$

where T^{DSO}_{sh}, T^{EVA}_{sh}, and T^{LA}_{sh} are the individual scheduling horizons of DSO, EVA, and LA, respectively.

2) Next, evaluate the scheduling potential of agents within the designated scheduling horizon using the aggregation method. To avoid exorbitant numbers of new variables and constraints generated during the aggregation process of individual models, a Minkowski-sum based aggregation method is applied to assess the scheduling potential of EVA (i. e., power flexibility of EVA).

The main idea is that the power flexibility model of each EV can be represented by a convex polytope with its corresponding Euclidean space representing the feasible power scheduling region, as shown in Fig. 4. The Minkowski-sum of multiple polytopes can be obtained by summing their vertex pairs and eliminating redundant points from the result [25]. The aggregated scheduling region obtained in this manner can maintain the power scheduling constraints of individual EVs while reducing variable dimensions. As an individual EV takes its charging power in each time interval as a decision variable, the Minkowski-sum of individual power flexibility models requires a consistent aggregation time window across all EVs. The time definition domain of individual power flexibility models is extended from their active state to the designated scheduling horizon to account for the differences in availability of EVs. With the rolling scheduling and control horizons, the scheduling potential of EVA is also dynamically evaluated. It should be noted that the Minkowski-sum based aggregation method is also applicable to other types of schedulable devices, e.g., flexible loads in [25] and [26].

3) Then, the scheduling potentials of agents are fed to the cooperative scheduling models of DSO, EVA, and LA. The carbon cost is incorporated into the decision-making models to pursue the maximum energy savings and carbon reductions while maximizing the economic benefits of all involved agents. Here, the carbon reduction is attained through load transferring and V2G services. The electricity and carbon trading among agents is achieved via Nash bargaining, and the optimal scheduling strategies are determined based on the Nash equilibrium (NE) [17]. To ensure the privacy of agents during trading, the cooperative scheduling model is solved using the ADMM algorithm in a distributed manner.

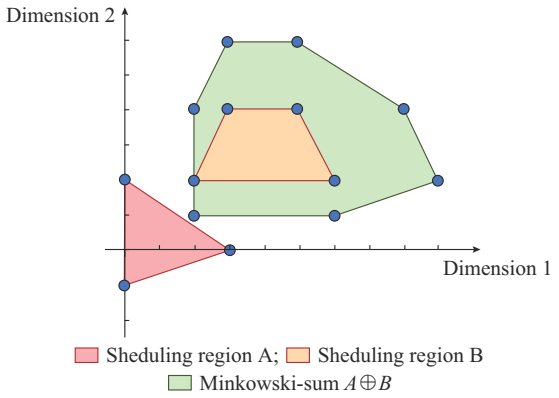

Fig. 4. Illustration of Minkowski-sum for two power scheduling regions.

4) Implement the optimal decision-making solution for the first interval of the scheduling horizon. Update the status of schedulable devices and then proceed to the next time instance ($t_r+\Delta t$) with the process above repeated, as shown in Fig. 2.

III. Evaluation on Sceduling Potential of EVA

Depending on the selected charging method, the charging power of an EV typically falls within the range of 2-120 kW, which does not qualify for entering the wholesale market [27]. To participate in a joint scheduling with DSO, EVAs act as the intermediary between EVs and DSO, capable of simultaneously managing multiple CSs while maintaining the communication with DSO. To maximize the revenues from V2G participation while fulfilling the charging requirements of EV users, it is essential to precisely evaluate the power flexibility of aggregated EVs.

A. Power Flexibility of Individual EV

For an EV connected to a V2G-supported CS, its power flexibility is mainly determined by the arrival battery SoC, the maximum allowed charging and discharging power, the expected departure time, and the minimum and maximum allowed battery SoCs. To simplify the analysis, the charging and discharging power losses are ignored. Thereby, the scheduling potential of an individual EV can be represented by:

$$\begin{cases} 0 \le P_{i,t}^{\mathrm{ev,c}} \le P_{i,\max}^{\mathrm{ev,c}} \quad t \in T_{i,\mathrm{a}} \\ 0 \le P_{i,t}^{\mathrm{ev,d}} \le P_{i,\max}^{\mathrm{ev,d}} \quad t \in T_{i,\mathrm{a}} \\ S_{i,t} = S_{i,t-1} + (P_{i,t}^{\mathrm{ev,c}} - P_{i,t}^{\mathrm{ev,d}})\Delta t / E_{i,\max}^{\mathrm{ev}} \\ S_i^{\min} \le S_{i,t} \le S_i^{\max} \quad t \in T_{i,\mathrm{a}} \\ P_{i,t}^{\mathrm{ev,c}} P_{i,t}^{\mathrm{ev,d}} = 0 \quad t \in T_{i,\mathrm{a}} \\ P_{i,t}^{\mathrm{ev,c}} = 0 \quad t \notin T_{i,\mathrm{a}} \\ P_{i,t}^{\mathrm{ev,d}} = 0 \quad t \notin T_{i,\mathrm{a}} \end{cases} \tag{5}$$

where $P_{i,t}^{\mathrm{ev,c}}$ and $P_{i,t}^{\mathrm{ev,d}}$ are the charging and discharging power for the i^{th} EV at time t, respectively, with its battery SoC represented by $S_{i,t}$; and $S_i^{\min}$ and $S_i^{\max}$ are the minimum and maximum allowed battery SoCs, respectively.

B. Power Flexibility of Aggregated EVs

To align with the cooperative scheduling based on rolling-horizon control framework, as introduced in Section II, the power flexibility of aggregated EVs should be consecutively evaluated as time progresses. The scheduling horizon of EVA for a given time instance is determined by the number of EVs being charged and their remaining charging periods, as mentioned in (1)-(3). Subsequently, the individual power flexibility models of available EVs can be established by (5). Given that directly incorporating individual power flexibility models into the scheduling model introduces excessive variables and constraints, the Minkowski-sum based aggregation method is applied to evaluate the power flexibility of aggregated EVs.

As clarified in Section II, the Minkowski-sum based aggregation method requires that all available EVs have their individual power flexibility models featured by the same definition domain (i.e., the same aggregation time window). The availability periods of EVs (i.e., $T_{i,\mathrm{a}}$ in (2)) have to be expanded to the scheduling horizon T_{sh}. To achieve this, a binary variable $u_{i,t}$ is introduced, which indicates the charging state of the i^{th} EV at time t, as in (6). Afterwards, the original individual power flexibility model can be reformatted as (7), with its time horizon expanded from $T_{i,\mathrm{a}}$ to T_{sh} ($T_{i,\mathrm{a}} \in T_{\mathrm{sh}}$). With the expanded time horizon of individual power flexibility models, the power flexibility of aggregated EVs can be computed using the Minkowski-sum based aggregation method, as in (8). This method not only preserves privacy of EV owners but also reduces the variable dimensions in the subsequent collaborative optimization stages.

$$u_{i,t} = \begin{cases} 1 & t \in T_{i,\mathrm{a}} \\ 0 & t \notin T_{i,\mathrm{a}} \end{cases} \tag{6}$$

$$\begin{cases} 0 \le P_{i,t}^{\mathrm{ev,c}} \le u_{i,t} P_{i,\max}^{\mathrm{ev,c}} \quad t \in T_{\mathrm{sh}} \\ 0 \le P_{i,t}^{\mathrm{ev,d}} \le u_{i,t} P_{i,\max}^{\mathrm{ev,d}} \quad t \in T_{\mathrm{sh}} \\ E_{i,t} = E_{i,t-1} + E_i^{\mathrm{ar}} u_{i,t}(u_{i,t} - u_{i,t-1}) - E_i^{\mathrm{ex}} u_{i,t-1}(u_{i,t-1} - u_{i,t}) + \\ \qquad (P_{i,t}^{\mathrm{ev,c}} - P_{i,t}^{\mathrm{ev,d}})\Delta t \quad t \in T_{\mathrm{sh}} \\ u_{i,t} E_i^{\min} \le E_{i,t} \le u_{i,t} E_i^{\max} \quad t \in T_{\mathrm{sh}} \end{cases} \tag{7}$$

$$\begin{cases} 0 \le P_{v,t}^{\mathrm{ev,c}} \le P_{v,t}^{\mathrm{c,max}} \quad t \in T_{\mathrm{sh}} \\ 0 \le P_{v,t}^{\mathrm{ev,d}} \le P_{v,t}^{\mathrm{d,max}} \quad t \in T_{\mathrm{sh}} \\ E_{v,t} = E_{v,t-1} + P_{v,t}^{\mathrm{ev,c}} \Delta t - P_{v,t}^{\mathrm{ev,d}} \Delta t + \Delta E_{v,t} \quad t \in T_{\mathrm{sh}} \\ \Delta E_{v,t} = \sum_{i \in I_v} [(u_{i,t}^2 - u_{i,t} u_{i,t-1}) E_i^{\mathrm{ar}} - (u_{i,t-1}^2 - u_{i,t-1} u_{i,t}) E_i^{\mathrm{ex}}] \quad t \in T_{\mathrm{sh}} \\ E_{v,t}^{\min} \le E_{v,t} \le E_{v,t}^{\max} \quad t \in T_{\mathrm{sh}} \end{cases} \tag{8}$$

where $E_{i,t}$ is the battery capacity of the i^{th} EV at time t, and it is subjected to $E_{i,t} = S_{i,t} E_{i,\max}^{\mathrm{ev}}$; $E_i^{\min}$ and $E_i^{\max}$ are the allowed minimum and maximum values of $E_{i,t}$, respectively; E_i^{ar} and E_i^{ex} are the arrival and departure battery capacities of the i^{th} EV, respectively; $P_{v,t}^{\mathrm{ev,c}}$ and $P_{v,t}^{\mathrm{ev,d}}$ are the aggregated charging and discharging power of the v^{th} EV cluster at time t, respectively, and $P_{v,t}^{\mathrm{c,max}}$ and $P_{v,t}^{\mathrm{d,max}}$ are their corresponding maximum values; and $E_{v,t}$ is the aggregated battery capacity while its step change is represented by $\Delta E_{v,t}$.

IV. Multi-agent Decision-making Models Considering Cooperative Carbon Reduction Potential

In this section, the decision-making models of tripartite agents, namely, DSO, LA, and EVA, are introduced, aiming

at obtaining cooperative low-carbon economic scheduling.

A. Decision-making Model of DSO

DSO adopts a carbon trading mechanism to regulate the output of carbon-emission power generation units, aiming to maximize its profit, which is the difference between the revenue from electricity sales and the operating costs. The revenue of DSO C^{DSO} comes from selling electricity to LA and EVA at high market prices, with the corresponding revenues represented by $C_{\mathrm{s}}^{\mathrm{LA}}$ and $C_{\mathrm{s}}^{\mathrm{EVA}}$, respectively. The operating costs of DSO include the cost of power purchased from transmission systems, the operating cost of GTGs, and the carbon cost, denoted by C^{G}, C^{TH}, and $C_{\mathrm{m}}^{\mathrm{TH}}$, respectively. The objective function for decision-making model of DSO is represented by (9) and detailed in (10). This paper applies free carbon quota allocation to GTGs, with their carbon emissions and allocated carbon quota represented by (11).

$$\max C^{\mathrm{DSO}} = C_{\mathrm{s}}^{\mathrm{LA}} + C_{\mathrm{s}}^{\mathrm{EVA}} - C^{\mathrm{G}} - C^{\mathrm{TH}} - C_{\mathrm{m}}^{\mathrm{TH}} \tag{9}$$

$$\begin{cases} C_{\mathrm{s}}^{\mathrm{EVA}} = \sum_{t}\sum_{v\in V} c_{v,t}^{\mathrm{cd}}\left(P_{v,t}^{\mathrm{ev,c}} - P_{v,t}^{\mathrm{ev,d}}\right) \\ C_{\mathrm{s}}^{\mathrm{LA}} = \sum_{t} c_t^{\mathrm{l}} P_{j,t}^{\mathrm{la}} \\ C^{\mathrm{G}} = \sum_{t} c_t^{\mathrm{g}} P_{j,t}^{\mathrm{g}} \\ C^{\mathrm{TH}} = \sum_{t}\sum_{h\in H}\left[a_h\left(P_{j,h,t}^{\mathrm{th}}\right)^2 + b_h P_{j,h,t}^{\mathrm{th}} + c_h\right] \\ C_{\mathrm{m}}^{\mathrm{TH}} = \sum_{t}\sum_{h\in H} c^{\mathrm{th}}\left(E_{j,h,t}^{\mathrm{q}} - E_{j,h,t}^{\mathrm{p}} + E_{j,h,t}^{\mathrm{g}}\right) \end{cases} \tag{10}$$

$$\begin{cases} E_{j,h,t}^{\mathrm{q}} = \delta_h P_{j,h,t}^{\mathrm{th}} \\ E_{j,h,t}^{\mathrm{p}} = \varsigma_h P_{j,h,t}^{\mathrm{th}} \\ E_{j,h,t}^{\mathrm{g}} = \delta_g P_{j,t}^{\mathrm{g}} \end{cases} \tag{11}$$

where v and h are the indices of the EV cluster and GTG, whose sets are represented by V and H, respectively; $c_{v,t}^{\mathrm{cd}}$ and c_t^{l} are the electricity selling prices to EVA and LA, respectively; c_t^{g} is the time-of-use (TOU) electricity price; $P_{j,t}^{\mathrm{la}}$ and $P_{j,t}^{\mathrm{g}}$ are the basic power demand of LA and purchased power of DSO at time t, respectively; a_h, b_h, and c_h are the operating cost coefficients; c^{th} is the unit carbon price; $P_{j,h,t}^{\mathrm{th}}$, $E_{j,h,t}^{\mathrm{q}}$ and $E_{j,h,t}^{\mathrm{p}}$ are the power output, carbon emission, and carbon emission quota, respectively; $E_{j,h,t}^{\mathrm{g}}$ is the carbon emission quota purchased from transmission systems; δ_h and ς_h are the carbon emission coefficient and the coefficient of carbon quota allocation, respectively; δ_g is the coefficient of indirect carbon emissions from power purchase; and $t \in T_{\mathrm{sh}}$.

Apart from maximizing profit, DSO is responsible for ensuring the integrity of the distribution network [28]. Any scheduling scheme that leads to network congestion or power imbalance is considered as an infeasible one. Therefore, the decision-making solutions of DSO must satisfy the network security constraints, which are further divided into the nodal power balance constraint, the system power constraint, and the branch flow constraint, as indicated by (12)-(14), respectively.

$$P_{ij,t} - \sum_{o:j\to o} P_{jo,t} + \sum_{h} P_{j,h,t}^{\mathrm{th}} + P_{j,t}^{\mathrm{re}} = P_{j,t}^{\mathrm{la}} + P_{j,v,t}^{\mathrm{ev,c}} - P_{j,t}^{\mathrm{ev,d}} \tag{12}$$

$$\sum_{\varsigma:0\to i} P_{0i,t} = P_{0,t}^{\mathrm{g}} \tag{13}$$

$$0 \le P_{ij,t} \le P_{ij}^{\max} \tag{14}$$

where $P_{ij,t}$ is the branch power flow between node j and its adjacent upstream node i; $P_{jo,t}$ is the branch power flow between node j and its adjacent downstream node o; $P_{ij}^{\max}$ is the security limit of $P_{ij,t}$; $P_{j,t}^{\mathrm{re}}$ is the total power output of DGs at node j; $P_{0,t}^{\mathrm{g}}$ and $P_{0i,t}$ are the power purchased from transmission systems and the power supplied to the adjacent downstream nodes of the slack bus, respectively; $\sigma: j\to o$ represents the adjacent downstream node sets of node j; ζ: $0\to i$ represents the adjacent downstream node sets of the slack bus; and $t \in T_{\mathrm{sh}}$.

In addition, the operating constraints of DSO and its flexible devices should also be considered during electricity and carbon trading. Specifically, the power purchased from transmission systems by DSO must be kept below its upper limit, as in (15). The power scheduling of GTGs and renewable generation systems has to obey their operating constraints, as in (16) and (17), respectively.

$$0 \le P_{j,t}^{\mathrm{g}} \le P_{\max}^{\mathrm{g}} \tag{15}$$

$$\begin{cases} -R_h^{\mathrm{dw}} \le P_{h,t}^{\mathrm{th}} - P_{h,t-1}^{\mathrm{th}} \le R_h^{\mathrm{up}} \\ P_{h,t}^{\mathrm{th,min}} \le P_{h,t}^{\mathrm{th}} \le P_{h,t}^{\mathrm{th,max}} \end{cases} \tag{16}$$

$$0 \le P_{j,t}^{\mathrm{re}} \le P_t^{\mathrm{r}} \tag{17}$$

where $P_{j,t}^{\mathrm{g}}$ is the power purchased from transmission systems, with its upper limit represented by $P_{\max}^{\mathrm{g}}$; R_h^{up} and R_h^{dw} are the maximum allowed ramp-up and ramp-down rates of the h^{th} GTG, respectively, and $P_{h,t}^{\mathrm{th,min}}$ and $P_{h,t}^{\mathrm{th,max}}$ are the corresponding minimum and maximum allowed power outputs; $P_{j,t}^{\mathrm{re}}$ is the total power output of DGs at node j with its predicted maximum value represented by P_t^{r}; and $t \in T_{\mathrm{sh}}$.

B. Decision-making Model of LA

As an intermediary linking consumers and DSO, LA defines the optimal scheduling schemes based on the TOU electricity price [29]. All flexible loads are motivated to optimize their consumption profiles to receive proper remuneration. LA aims to maximize the user surplus C^{LA}, which is the difference between the utility function and electricity cost of consumers. The utility of consumers in this context refers to the satisfaction derived from electricity consumption and is represented by the commonly used quadratic utility function introduced in [30]. The operating constraint of LA is given in (20).

$$\max C^{\mathrm{LA}} = F_{\mathrm{u}} - C_{\mathrm{b}}^{\mathrm{LA}} \tag{18}$$

$$F_{\mathrm{u}} = \sum_{t}\left[\alpha_{\mathrm{e}} P_t^{\mathrm{la}} - \frac{\beta_{\mathrm{e}}}{2}\left(P_t^{\mathrm{la}}\right)^2\right] \tag{19}$$

$$\begin{cases} \sum_{t} P_{\mathrm{tran},t} = 0 \\ \left| P_{\mathrm{tran},t} \right| \le \varpi P_t^{\mathrm{la}'} \\ P_t^{\mathrm{la}} = P_t^{\mathrm{la}'} + P_{\mathrm{tran},t} \end{cases} \tag{20}$$

where F_{u} is the utility function of consumers, which measures the satisfaction degree of consumers; $C_{\mathrm{b}}^{\mathrm{LA}}$ is the electricity cost of LA, which equals the electricity selling reve-

nue of DSO, i.e., $C_{\mathrm{b}}^{\mathrm{LA}}=C_{\mathrm{s}}^{\mathrm{LA}}$; α_{e} and β_{e} are the preference coefficients of consumers; $P_{\mathrm{tran},t}$ and $P_t^{\mathrm{la}'}$ are the transferable and baseline load power of LA, respectively; P_t^{la} is the total power demand of LA; ϖ is the transferable power ratio; and $t\in T_{\mathrm{sh}}$.

C. Decision-making Model of EVA

To motivate EVs to provide V2G service and engage in the carbon trading market, EVA is assumed to get revenues by selling its equivalent carbon quota in the carbon trading market. Meanwhile, EVA tends to minimize its electricity cost while meeting the charging demands of EVs. Therefore, the control objective of EVA is to maximize the difference between carbon quota trading revenue and electricity cost, as in (21). As the EV charging scheduling must prioritize meeting the charging demands of EVs, the power flexibility of aggregated EVs defined in (8) is applied as the operating constraint of EVA.

$$\max C^{\mathrm{EVA}}=C_{\mathrm{m}}^{\mathrm{EVA}}-C_{\mathrm{b}}^{\mathrm{EVA}} \tag{21}$$

$$C_{\mathrm{m}}^{\mathrm{EVA}}=\sum_t\sum_v c^{\mathrm{th}}(L^{\mathrm{ev}}E^{\mathrm{gas}}-E^{\mathrm{net}})(P_{v,t}^{\mathrm{ev,c}}-P_{v,t}^{\mathrm{ev,d}}) \tag{22}$$

where C^{EVA} is the benefit of EVA; $C_{\mathrm{b}}^{\mathrm{EVA}}$ and $C_{\mathrm{m}}^{\mathrm{EVA}}$ are the electricity cost and carbon quota trading revenue of EVA, respectively, and in a cooperative game, the electricity cost of EVA equals the electricity sales revenue of DSO, i.e., $C_{\mathrm{b}}^{\mathrm{EVA}}=C_{\mathrm{s}}^{\mathrm{EVA}}$; E^{gas} is the carbon emission of gasoline vehicles per km; L^{ev} is the equivalent travelling distance of gasoline vehicles per kWh; and E^{net} is the carbon emission from EV charging.

V. Source–Load–Storage Cooperative Low-carbon Scheduling Model and Its Distributed Solving Algorithm

Based on the decision-making models of DSO, LA, and EVA, their cooperative scheduling model can be established and described as a Nash game in this section, with the optimal solution determined by NE. Meanwhile, the ADMM algorithm in the distributed manner is applied to preserve data privacy of the three agents.

A. Nash Bargaining Based Cooperative Scheduling Model

The Nash bargaining theory in cooperative games can enhance the interests of all agents without sacrificing their interests [17]. Hence, both competition and cooperation exist among the involved agents. A fair and reasonable equilibrium solution can be achieved through negotiation, representing the optimal Pareto solution for all cooperative agents. To ensure the existence of the NE point during the multi-agent coordination, it is assumed that each agent acts independently and rationally in pursuit of the maximum profits. Once all the three agents reach a consensus through negotiation, they can engage in the electricity and carbon trading, benefiting all agents involved. The Nash product is applied to ensure fair benefit distribution among all self-interested agents, and the complete Nash bargaining based cooperative scheduling model is formulated as:

$$\begin{cases}\max(C^{\mathrm{DSO}}-C_{0,*}^{\mathrm{DSO}})(C^{\mathrm{LA}}-C_{0,*}^{\mathrm{LA}})(C^{\mathrm{EVA}}-C_{0,*}^{\mathrm{EVA}})\\ \text{s.t. } C^{\mathrm{DSO}}\ge C_{0,*}^{\mathrm{DSO}}\\ \quad C^{\mathrm{LA}}\ge C_{0,*}^{\mathrm{LA}}\\ \quad C^{\mathrm{EVA}}\ge C_{0,*}^{\mathrm{EVA}}\\ \quad (8),\ (12)\text{-}(17),\ (20)\end{cases} \tag{23}$$

where $C_{0,*}^{\mathrm{DSO}}$, $C_{0,*}^{\mathrm{LA}}$, and $C_{0,*}^{\mathrm{EVA}}$ are the benefits of DSO, LA, and EVA before bargaining (i.e., the disagreement points), respectively; and $C-C_{0,*}$ (with the subscript omitted for simplicity) is the increased benefit of each agent after Nash bargaining.

B. Equivalent Transformation of Nash Bargaining Based Cooperative Scheduling Model

The Nash bargaining based cooperative scheduling model in (23) is a nonconvex and nonlinear optimization problem, which poses challenges for direct problem-solving. Also, this model has a centralized structure and necessitates agents to share their individual information, raising privacy concerns. The Nash bargaining based cooperative scheduling model will be decomposed and decoupled in this subsection to address the issues above. Based on the mean value theorem, the essential conditions for an optimal solution in a mean-value inequality are "positive, definite, and equal". As for the model in (23), the justification for the existence of a Pareto optimal equilibrium is as follows.

1) Positive: as the Nash bargaining based cooperative scheduling model is intended to promote the interests of all participants, it is reasonable to expect the existence of scheduling strategies that lead to a positive value of (23).

2) Definite: the sum of increased benefits of three agents is expressed as $C^{\mathrm{DSO}}+C^{\mathrm{LA}}+C^{\mathrm{EVA}}-(C_{0,*}^{\mathrm{DSO}}+C_{0,*}^{\mathrm{LA}}+C_{0,*}^{\mathrm{EVA}})$. Since the disagreement points $C_{0,*}^{\mathrm{DSO}}$, $C_{0,*}^{\mathrm{LA}}$, and $C_{0,*}^{\mathrm{EVA}}$ are definite values, the maximization of the objective function in (23) is equivalent to the maximization of $C^{\mathrm{DSO}}+C^{\mathrm{LA}}+C^{\mathrm{EVA}}$, as illustrated in (24).

$$\begin{aligned}&\max(C^{\mathrm{DSO}}-C_{0,*}^{\mathrm{DSO}})(C^{\mathrm{LA}}-C_{0,*}^{\mathrm{LA}})(C^{\mathrm{EVA}}-C_{0,*}^{\mathrm{EVA}})\Leftrightarrow\\ &\quad\max(C^{\mathrm{DSO}}+C^{\mathrm{LA}}+C^{\mathrm{EVA}})\Leftrightarrow\\ &\quad\max(C_{\mathrm{s}}^{\mathrm{LA}}+C_{\mathrm{s}}^{\mathrm{EVA}}-C^{\mathrm{G}}-C^{\mathrm{TH}}-C_{\mathrm{m}}^{\mathrm{TH}}+F_{\mathrm{u}}-C_{\mathrm{b}}^{\mathrm{LA}}+\\ &\quad C_{\mathrm{m}}^{\mathrm{EVA}}-C_{\mathrm{b}}^{\mathrm{EVA}})\Leftrightarrow\max(Z_{\mathrm{DSO}}+F_{\mathrm{u}}+C_{\mathrm{m}}^{\mathrm{EVA}})\end{aligned} \tag{24}$$

where $Z_{\mathrm{DSO}}=-C^{\mathrm{G}}-C^{\mathrm{TH}}-C_{\mathrm{m}}^{\mathrm{TH}}$.

3) Equal: the arithmetic-geometric mean (AM-GM) inequality states that the geometric mean of any list of nonnegative real values is less than or equal to its arithmetic mean, as in (25).

$$\begin{aligned}&\sqrt[n]{x_1x_2\ldots x_n}\le\frac{x_1+x_2+\ldots+x_n}{n}\Leftrightarrow\\ &\quad x_1x_2\ldots x_n\le\left(\frac{x_1+x_2+\ldots+x_n}{n}\right)^n\end{aligned} \tag{25}$$

where $x_1,x_2,\ldots,x_n$ are the nonnegative real values, and n is their total number. The equal sign in (25) holds when $x_1=x_2=\ldots=x_n$.

According to the AM-GM inequality, the model in (23) satisfies (26), and the inequality takes the equal sign if and only if (27) holds. By substituting the definitions of C^{DSO}, C^{LA}, and C^{EVA} as provided in (9), (18), and (21), respectively, (28) can be derived and considered the prerequisite for at-

taining the maximum value of the objective function in (23). It is worth noting that when the objective function of the Nash bargaining based cooperative scheduling model is maximized, the resulting solution ensures that all participating agents achieve Pareto optimal benefits, thereby entering into a Pareto optimal equilibrium, the proof of which can be found in [31].

$$(C^{\mathrm{DSO}}-C_{0,*}^{\mathrm{DSO}})(C^{\mathrm{LA}}-C_{0,*}^{\mathrm{LA}})(C^{\mathrm{EVA}}-C_{0,*}^{\mathrm{EVA}})\le [(C^{\mathrm{DSO}}-C_{0,*}^{\mathrm{DSO}}+C^{\mathrm{LA}}-C_{0,*}^{\mathrm{LA}}+C^{\mathrm{EVA}}-C_{0,*}^{\mathrm{EVA}})/3]^3 \tag{26}$$

$$C^{\mathrm{DSO}}-C_{0,*}^{\mathrm{DSO}}=C^{\mathrm{LA}}-C_{0,*}^{\mathrm{LA}}=C^{\mathrm{EVA}}-C_{0,*}^{\mathrm{EVA}} \tag{27}$$

$$Z_{\mathrm{DSO}}+C_{\mathrm{s}}^{\mathrm{LA}}+C_{\mathrm{s}}^{\mathrm{EVA}}-C_{0,*}^{\mathrm{DSO}}=F_{\mathrm{u}}-C_{\mathrm{b}}^{\mathrm{LA}}-C_{0,*}^{\mathrm{LA}}=C_{\mathrm{m}}^{\mathrm{EVA}}-C_{\mathrm{b}}^{\mathrm{EVA}}-C_{0,*}^{\mathrm{EVA}}=(Z_{\mathrm{DSO}}+F_{\mathrm{u}}+C_{\mathrm{m}}^{\mathrm{EVA}}-C_{0,*}^{\mathrm{DSO}}-C_{0,*}^{\mathrm{LA}}-C_{0,*}^{\mathrm{EVA}})/3 \tag{28}$$

After applying the above equivalent transformation, the model in (23) can be divided into sub-problems 1 and 2. The Pareto solution of the model in (23) can be achieved by solving these two sub-problems in sequence.

1) Sub-problem 1: Maximizing Benefit of Cooperative Agents

$$\begin{cases}\max(Z_{\mathrm{DSO}}+F_{\mathrm{u}}+C_{\mathrm{m}}^{\mathrm{EVA}})\\ \text{s.t. } Z_{\mathrm{DSO}}=-C^{\mathrm{G}}-C^{\mathrm{TH}}-C_{\mathrm{m}}^{\mathrm{TH}}\\ \quad C_{\mathrm{s}}^{\mathrm{LA}}=C_{\mathrm{b}}^{\mathrm{LA}}\\ \quad C_{\mathrm{s}}^{\mathrm{EVA}}=C_{\mathrm{b}}^{\mathrm{EVA}}\\ \quad (8),\ (12)\text{-}(17),\ (20)\end{cases} \tag{29}$$

It is noticed that (29) is a typical planning problem and can be solved directly using commercial optimization solvers. However, the centralized problem-solving of (29) may raise privacy concerns for the agents.

2) Sub-problem 2: Profit Distribution for Electricity and Carbon Trading

$$\begin{cases}\max (C_{\mathrm{s}}^{\mathrm{LA}}+C_{\mathrm{s}}^{\mathrm{EVA}}+Z_{\mathrm{DSO}}^{*}-C_{0,*}^{\mathrm{DSO}})(F_{\mathrm{u}}^{*}-C_{\mathrm{b}}^{\mathrm{LA}}-C_{0,*}^{\mathrm{LA}})\cdot\\ \quad (C_{\mathrm{m}}^{\mathrm{EVA}*}-C_{\mathrm{b}}^{\mathrm{EVA}}-C_{0,*}^{\mathrm{EVA}})\\ \text{s.t. } C_{\mathrm{s}}^{\mathrm{LA}}+C_{\mathrm{s}}^{\mathrm{EVA}}+Z_{\mathrm{DSO}}^{*}\ge C_{0,*}^{\mathrm{DSO}}\\ \quad F_{\mathrm{u}}^{*}-C_{\mathrm{b}}^{\mathrm{LA}}\ge C_{0,*}^{\mathrm{LA}}\\ \quad C_{\mathrm{m}}^{\mathrm{EVA}*}-C_{\mathrm{b}}^{\mathrm{EVA}}\ge C_{0,*}^{\mathrm{EVA}}\end{cases} \tag{30}$$

Utilizing the mean value theorem, (30) can be converted into a readily solvable equation, eliminating the need for a solver with the derivation process provided in (31). Formula (32) indicates that the cooperative alliance negotiations have reached a consensus on electricity and carbon trading, and the increased benefits are equally shared among the agents. The optimal solution of sub-problem 2 can be computed directly, as in (33).

$$\begin{aligned}&(C_{\mathrm{s}}^{\mathrm{LA}}+C_{\mathrm{s}}^{\mathrm{EVA}}+Z_{\mathrm{DSO}}^{*}-C_{0,*}^{\mathrm{DSO}})(F_{\mathrm{u}}^{*}-C_{\mathrm{b}}^{\mathrm{LA}}-C_{0,*}^{\mathrm{LA}})\cdot\\ &\quad (C_{\mathrm{m}}^{\mathrm{EVA}*}-C_{\mathrm{b}}^{\mathrm{EVA}}-C_{0,*}^{\mathrm{EVA}})\le[(Z_{\mathrm{DSO}}^{*}+C_{\mathrm{s}}^{\mathrm{LA}}+C_{\mathrm{s}}^{\mathrm{EVA}}-C_{0,*}^{\mathrm{DSO}}+F_{\mathrm{u}}^{*}-\\ &\quad C_{\mathrm{b}}^{\mathrm{LA}}-C_{0,*}^{\mathrm{LA}}+C_{\mathrm{m}}^{\mathrm{EVA}*}-C_{\mathrm{b}}^{\mathrm{EVA}}-C_{0,*}^{\mathrm{EVA}})]^3=\\ &\quad [(Z_{\mathrm{DSO}}^{*}-C_{0,*}^{\mathrm{DSO}}+F_{\mathrm{u}}^{*}-C_{0,*}^{\mathrm{LA}}-C_{\mathrm{m}}^{\mathrm{EVA}*}-C_{0,*}^{\mathrm{EVA}})/3]^3\end{aligned} \tag{31}$$

$$F_{\mathrm{u}}^{*}-C_{\mathrm{b}}^{\mathrm{LA}}-C_{0,*}^{\mathrm{LA}}=C_{\mathrm{m}}^{\mathrm{EVA}*}-C_{\mathrm{b}}^{\mathrm{EVA}}-C_{0,*}^{\mathrm{EVA}}=Z_{\mathrm{DSO}}^{*}+C_{\mathrm{s}}^{\mathrm{LA}}+C_{\mathrm{s}}^{\mathrm{EVA}}-C_{0,*}^{\mathrm{DSO}}=(Z_{\mathrm{DSO}}^{*}+F_{\mathrm{u}}^{*}+C_{\mathrm{m}}^{\mathrm{EVA}*}-C_{0,*}^{\mathrm{DSO}}-C_{0,*}^{\mathrm{LA}}-C_{0,*}^{\mathrm{EVA}})/3 \tag{32}$$

$$\begin{cases}C_{\mathrm{b}}^{\mathrm{LA}*}=-(Z_{\mathrm{DSO}}^{*}-2F_{\mathrm{u}}^{*}+C_{\mathrm{m}}^{\mathrm{EVA}*}-C_{0,*}^{\mathrm{DSO}}+2C_{0,*}^{\mathrm{LA}}-C_{0,*}^{\mathrm{EVA}})/3\\ C_{\mathrm{b}}^{\mathrm{EVA}*}=-(Z_{\mathrm{DSO}}^{*}+F_{\mathrm{u}}^{*}-2C_{\mathrm{m}}^{\mathrm{EVA}*}-C_{0,*}^{\mathrm{DSO}}-C_{0,*}^{\mathrm{LA}}+2C_{0,*}^{\mathrm{EVA}})/3\end{cases} \tag{33}$$

where Z_{DSO}^{*}, F_{u}^{*}, and $C_{\mathrm{m}}^{\mathrm{EVA}*}$ are the optimal solutions of sub-problem 1; and the equality in (31) is satisfied only when (32) exits.

C. ADMM Algorithm in Distributed Manner

To maintain the operational autonomy and information privacy of agents, sub-problem 1 is solved by the ADMM algorithm in a distributed manner. As the ADMM algorithm requires the optimization model to be decomposable, the auxiliary variables are used to facilitate the model decoupling (i.e., $P_{\mathrm{s},t}^{\mathrm{la}}=P_{\mathrm{b},t}^{\mathrm{la}}$, $P_{\mathrm{s},v,t}^{\mathrm{ev}}=P_{\mathrm{b},v,t}^{\mathrm{ev}}$, where $P_{v,t}^{\mathrm{ev}}=P_{v,t}^{\mathrm{ev,c}}-P_{v,t}^{\mathrm{ev,d}}$). By incorporating these auxiliary variables and taking the negative form of (29), the augmented Lagrangian function of sub-problem 1 can be formulated, as in (34).

$$\begin{aligned}\min L=&-(Z_{\mathrm{DSO}}+F_{\mathrm{u}}+C_{\mathrm{m}}^{\mathrm{EVA}})+\\ &\sum_{t}\left\{\lambda_{t}^{\mathrm{la}}(P_{\mathrm{s},t}^{\mathrm{la}}-P_{\mathrm{b},t}^{\mathrm{la}})+\frac{\rho_{\mathrm{la}}}{2}\left\|P_{\mathrm{s},t}^{\mathrm{la}}-P_{\mathrm{b},t}^{\mathrm{la}}\right\|_2^2+\right.\\ &\left.\sum_{v}\left[\lambda_{t}^{\mathrm{ev}}(P_{\mathrm{s},v,t}^{\mathrm{ev}}-P_{\mathrm{b},v,t}^{\mathrm{ev}})+\frac{\rho_{\mathrm{ev}}}{2}\left\|P_{\mathrm{s},v,t}^{\mathrm{ev}}-P_{\mathrm{b},v,t}^{\mathrm{ev}}\right\|_2^2\right]\right\}\end{aligned} \tag{34}$$

where λ_t^{la} and λ_t^{ev} are the Lagrangian multipliers of LA and EVA at time t, respectively; and ρ_{la} and ρ_{ev} are the penalty factors of LA and EVA, respectively.

Formula (34) can be deconstructed into the corresponding distributed optimization models for LA, EVA, and DSO, as in (35)-(37), respectively.

1) Distributed optimization model for LA

$$\begin{cases}\min L_{\mathrm{LA}}=-F_{\mathrm{u}}+\sum_{t}\left[\lambda_{t}^{\mathrm{la}}(P_{\mathrm{s},t}^{\mathrm{la}}-P_{\mathrm{b},t}^{\mathrm{la}})+\frac{\rho_{\mathrm{la}}}{2}\left\|P_{\mathrm{s},t}^{\mathrm{la}}-P_{\mathrm{b},t}^{\mathrm{la}}\right\|_2^2\right]\\ \text{s.t. } (20)\end{cases} \tag{35}$$

2) Distributed optimization model for EVA

$$\begin{cases}\min L_{\mathrm{EVA}}=\sum_{t}\sum_{v}\left[\lambda_{t}^{\mathrm{ev}}(P_{\mathrm{s},v,t}^{\mathrm{ev}}-P_{\mathrm{b},v,t}^{\mathrm{ev}})+\frac{\rho_{\mathrm{ev}}}{2}\left\|P_{\mathrm{s},v,t}^{\mathrm{ev}}-P_{\mathrm{b},v,t}^{\mathrm{ev}}\right\|_2^2\right]-\\ \qquad C_{\mathrm{m}}^{\mathrm{EVA}}\\ \text{s.t. } (8)\end{cases} \tag{36}$$

3) Distributed optimization model for DSO

$$\begin{cases}\min L_{\mathrm{DSO}}=-Z_{\mathrm{DSO}}+\sum_{t}\left\{\lambda_{t}^{\mathrm{la}}(P_{\mathrm{s},t}^{\mathrm{la}}-P_{\mathrm{b},t}^{\mathrm{la}})+\frac{\rho_{\mathrm{la}}}{2}\left\|P_{\mathrm{s},t}^{\mathrm{la}}-P_{\mathrm{b},t}^{\mathrm{la}}\right\|_2^2+\right.\\ \qquad\left.\sum_{v}\left[\lambda_{t}^{\mathrm{ev}}(P_{\mathrm{s},v,t}^{\mathrm{ev}}-P_{\mathrm{b},v,t}^{\mathrm{ev}})+\frac{\rho_{\mathrm{ev}}}{2}\left\|P_{\mathrm{s},v,t}^{\mathrm{ev}}-P_{\mathrm{b},v,t}^{\mathrm{ev}}\right\|_2^2\right]\right\}\\ \text{s.t. } (12)\text{-}(17)\end{cases} \tag{37}$$

Due to the existence of discrete and bilinear terms, (35)-(37) are further linearized to mixed-integer linear programming (MILP) problems before being fed to the ADMM solving procedure. This step enables the commercial integer optimization solvers to solve the MILP problems. The linearization technique has been extensively explored in the existing literature [32], [33] and will not be repeated here. In addition to using the linearization technique, various machine learning techniques have been applied in the existing literature to enhance the traditional ADMM (e. g., Q-learning in [34] and deep neural networks in [35]). The incorporation of either linearization or machine learning techniques into ADMM will not affect the effectiveness of the proposed source–load–storage low-carbon cooperative scheduling strategy.

The linearized sub-problem 1 can be solved using the ADMM algorithm, with its implementation steps summarized below.

Step 1: apply the basic settings for the ADMM algorithm (the maximum iteration number $k_{\max}=50$; the convergence tolerance $\delta=10^{-5}$; and the penalty factor $\rho=10^{-4}$).

Step 2: initialize the iteration number k and the Lagrangian multipliers λ_k to be 0; and initialize the power purchase of LA and EVA to be 0 (i.e., $P_t^{\mathrm{la},k}=P_{v,t}^{\mathrm{ev},k}=0$).

Step 3: based on the power supply from DSO to LA and EVA at the k^{th} iteration, i.e., $P_{\mathrm{s},t}^{\mathrm{la},k}$ and $P_{\mathrm{s},v,t}^{\mathrm{ev},k}$, respectively, the expected power purchase of LA and EVA from DSO at the $(k+1)^{\mathrm{th}}$ iteration, i.e., $P_{\mathrm{b},t}^{\mathrm{la},k+1}$ and $P_{\mathrm{b},v,t}^{\mathrm{ev},k+1}$, respectively, can be computed, as in (38) and (39).

$$P_{\mathrm{b},t}^{\mathrm{la},k+1}=\arg\min L_{\mathrm{DSO}}^{k}(\lambda_t^{\mathrm{la},k},P_{\mathrm{s},t}^{\mathrm{la},k}) \tag{38}$$

$$P_{\mathrm{b},v,t}^{\mathrm{ev},k+1}=\arg\min L_{\mathrm{EVA}}^{k}(\lambda_t^{\mathrm{ev},k},P_{\mathrm{s},v,t}^{\mathrm{ev},k}) \tag{39}$$

Step 4: after DSO receives $P_{\mathrm{b},t}^{\mathrm{la},k+1}$ and $P_{\mathrm{b},v,t}^{\mathrm{ev},k+1}$, they can be calculated by (40).

$$[P_{\mathrm{b},t}^{\mathrm{la},k+1},P_{\mathrm{b},v,t}^{\mathrm{ev},k+1}]=\arg\min L_{\mathrm{DSO}}^{k+1}(\lambda_t^{\mathrm{la},k},\lambda_t^{\mathrm{ev},k},P_{\mathrm{b},t}^{\mathrm{la},k+1},P_{\mathrm{b},v,t}^{\mathrm{ev},k+1}) \tag{40}$$

Step 5: update Lagrangian multipliers for LA and EVA, as shown in (41).

$$\begin{cases}\lambda_t^{\mathrm{la},k+1}=\lambda_t^{\mathrm{la},k}+\rho_{\mathrm{la}}(P_{\mathrm{s},t}^{\mathrm{la},k+1}-P_{\mathrm{b},t}^{\mathrm{la},k+1})\\ \lambda_t^{\mathrm{ev},k+1}=\lambda_t^{\mathrm{ev},k}+\rho_{\mathrm{ev}}(P_{\mathrm{s},v,t}^{\mathrm{ev},k+1}-P_{\mathrm{b},v,t}^{\mathrm{ev},k+1})\end{cases} \tag{41}$$

Step 6: send the updated parameters to the relevant distributed optimization models for LA and EVA.

Step 7: change the iteration number from k to $k+1$.

Step 8: repeat *Steps 3-7* until (42) is achieved or the maximum iteration number $k_{\max}$ is reached.

$$\begin{cases}\sum_t\left\|P_{\mathrm{s},t}^{\mathrm{la},k}-P_{\mathrm{b},t}^{\mathrm{la},k}\right\|_2^2\le\delta\\ \sum_t\left\|P_{\mathrm{s},v,t}^{\mathrm{ev},k}-P_{\mathrm{b},v,t}^{\mathrm{ev},k}\right\|_2^2\le\delta\end{cases} \tag{42}$$

Step 9: end the iteration and output the power transactions among the three agents.

VI. Case Study

A. Basic Information on System Under Test

The case study is performed on a modified Roy Billinton Test System (RBTS), with its single-line diagram depicted in Fig. 5 [36].

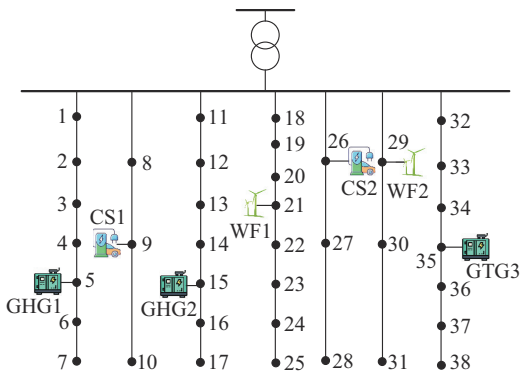

Fig. 5. Single-line diagram of modified RBTS.

The peak demand of the test network is 20 MW, and the power consumption profile of each node is provided in [37]. Additionally, two wind farms (WFs), each with a rated power of 6 MW, are integrated into the test network. The typical demand profile of baseline loads and the generation profiles of WFs are shown in Fig. 6.

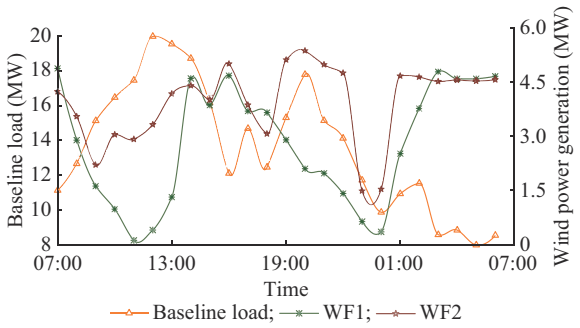

Fig. 6. Typical demand profile of baseline loads and generation profile of WFs.

Moreover, the response of agents to time-varying electricity prices is investigated using a TOU pricing method [38], which sets differentiated electricity prices for peak, off-peak, and valley periods, as tabulated in Table I. The transferrable power ratio ϖ is assumed to be 10%, while the preference coefficients of customers α_{e} and β_{e} are set to be 2.2 and 0.0009, respectively. For GTGs, the unit carbon price c^{th} and the carbon quota allocation coefficient ς_h are set to be 0.25 CNY/kg and 0.798 kg/kWh, respectively, with the other operating parameters specified in Table II. For decision-making model of EVA in (21) and (22), the equivalent carbon emission during the EV charging process E^{net} is set to be 0.5 kg/kWh, while the carbon emission of gasoline vehicles E^{gas} is set to be 0.197 kg/km. According to [39], a commercial EV with a battery capacity of 56.4 kWh can cover a driving range of 420 km. Hence, the equivalent travelling distance of gasoline vehicles per kWh, L^{ev}, is assumed to be 7 km. The upper and lower limits of electricity transaction price are 100% and 80% of the TOU electricity price, respectively.

TABLE I
TOU Electricity Price and Time Period Partition

Time period	Time period division	c_t^{g} (CNY/kWh)
Peak period	10:00-13:00, 18:00-22:00	1.25
Off-peak period	08:00-10:00, 13:00-18:00, 22:00-24:00	0.80
Valley period	00:00-08:00	0.40

TABLE II
Operating Parameters of GTGs

h	$P_{h,t}^{\mathrm{th,max}}$ (kW)	R_h^{up} (kW)	R_h^{dw} (kW)	(a_h,b_h,c_h)	δ_h
1	3000	3000	3000	(0.00018, 0.015, 0)	0.915
2	4000	3500	3500	(0.00015, 0.018, 0)	0.812
3	5000	4000	4000	(0.00022, 0.022, 0)	0.572

Two centralized CSs (CS1 and CS2) are accessible on the test network, catering to two types of EV charging: night-

time charging and daytime charging. To account for the variability and uncertainty of charging behaviors, the charging profiles of EV fleets are produced through Monte Carlo simulations, utilizing the presumed distribution characteristics of EV charging patterns given in Table III.

TABLE III
PROBABILITY DISTRIBUTIONS OF EV CHARGING PATTERNS

EV charging pattern	Probability distribution				
	Arrival time of EV to CS	$t_{i,\mathrm{ex}}$	$S_{i,\mathrm{ex}}$	Number of EVs on a daily basis	
				Served by CS1	Served by CS2
Nighttime charging	$N(20, 1)$	$N(8, 0.25)$	$U(0.3, 0.5)$	$U(460, 540)$	$U(280, 320)$
Daytime charging	$N(9, 1)$	$N(19, 1)$	$U(0.2, 0.4)$	$U(180, 220)$	$U(160, 240)$

Note: $N(x, y)$ stands for normal distribution; and $U(x, y)$ refers to uniform distribution.

The minimum and maximum allowable battery SoCs are set to be 0.1 and 0.95, respectively, assuming a battery capacity of 35 kWh. The maximum permissible charging power and discharging power are set to be 6.6 kW without considering the power conversion losses.

B. Results Analysis

1) Power Flexibility of Aggregated EVs

By applying the Minkowski-sum based aggregation method in a rolling-horizon control framework, the power flexibility of aggregated EVs for CS1 and CS2 on a typical day can be obtained, as shown in Fig. 7. It can be observed that CS1 and CS2 exhibit similar power flexibility of aggregated EVs. As the number of EVs being charged during 07: 00-10: 00 and 17:00-21:00 increases, the power and energy flexibilities of aggregated EVs are also enhanced. Due to more EVs getting charged during nighttime than daytime, the schedulable power of EV fleets is higher during nighttime.

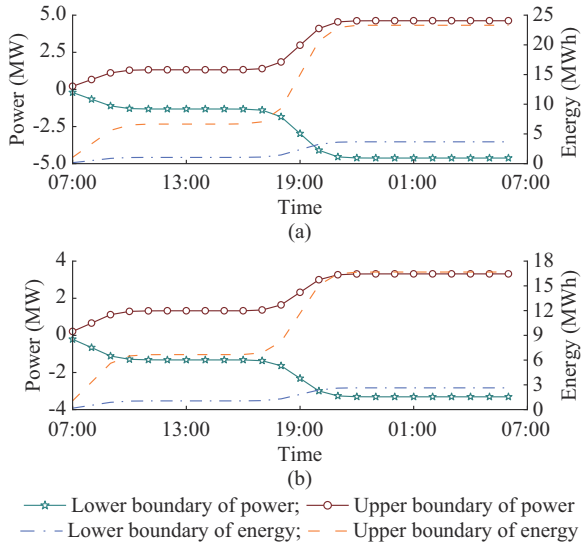

Fig. 7. Power and energy flexibility of aggregated EVs for CS1 and CS2. (a) CS1. (b) CS2.

2) Convergence Analysis of ADMM Algorithm for Sub-problem 1

As elucidated in Section V, the solution quality of sub-problem 1 is crucial for defining the cooperative scheduling schemes in sub-problem 2. To validate the convergence of sub-problem 1 using the ADMM algorithm, the iterative curves of the objective function values obtained from the distributed optimization models of DSO, LA, and EVA are shown in Fig. 8. It is clear that the distributed optimization models stabilize and converge after about 20 iterations. The objective function for each agent converges to NE in the ADMM algorithm. Throughout the entire process, only the information on buying and selling electricity is exchanged among agents. Once NE is reached, the scheduling strategies of all agents no longer change. This indicates that no agent can increase payoff by altering their scheduling strategies.

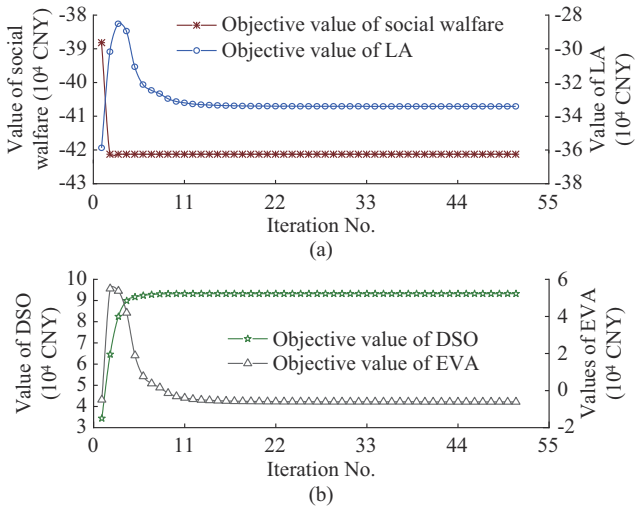

Fig. 8. Iterative curves of objective function values obtained from distributed optimization models. (a) LA and social welfare. (b) DSO and EVA.

3) Analysis of Optimization Results for Each Agent

The following three scheduling strategies are employed and compared to assess the effectiveness of the proposed one. All three strategies are implemented using the rolling-horizon control framework.

1) Strategy 1: the proposed low-carbon cooperative scheduling strategy.

2) Strategy 2: a centralized low-carbon scheduling strategy.

3) Strategy 3: a low-carbon scheduling strategy based on Stackelberg bargaining.

The implementation approaches of strategy 2 and strategy 3 can be found in [40] and [41], respectively. The optimized costs and revenues of the three agents are tabulated in Tables IV-VI. It turns out that DSO achieves the highest revenue under strategy 2, which focuses solely on maximizing the revenue of DSO without considering the revenues of other agents. Consequently, the electricity costs of LA and EVA increase while the costs of DSO decrease. Moreover, the user surplus of LA and net profit of EVA are the highest under strategy 1, as it reduces their energy costs and increases their revenues for both LA and EVA.

TABLE IV
OPTIMIZED COSTS AND REVENUES OF DSO

Strategy No.	Electricity sales revenue (10^4 CNY)	Operating cost of GTGs (10^4 CNY)	Carbon emission cost (10^4 CNY)	Electricity procurement cost (10^4 CNY)	Total cost (10^4 CNY)
1	18.3421	6.8917	0.3693	2.0617	9.3227
2	18.5592	6.9252	0.3642	2.0305	9.3199
3	18.2981	6.6986	0.4025	2.2673	9.3684

TABLE V
OPTIMIZED COSTS AND REVENUES OF LA

Strategy No.	User surplus (10^4 CNY)	Utility function of customers (10^4 CNY)	Electricity cost (10^4 CNY)
1	14.6285	42.1279	27.4994
2	14.4562	42.1265	27.6704
3	14.5882	42.0529	27.4647

TABLE VI
OPTIMIZED COSTS AND REVENUES OF EVA

Strategy No.	Net profit (10^4 CNY)	Carbon quota trading revenue (10^4 CNY)	Electricity cost (10^4 CNY)
1	0.4465	0.6081	0.1616
2	0.3993	0.6081	0.2088
3	0.4063	0.6081	0.2018

When comparing strategy 1 with strategy 3, the revenues of all agents increase, and the increments are equal, implying a balanced distribution of social benefits. Although the operating costs of GTGs are higher under strategy 1 than those under strategy 3, strategy 1 has lower carbon emission and electricity procurement costs.

It is due to the prioritization of low-carbon-emission GTGs and carbon-free EV discharging in strategy 1, despite the downside of higher operating costs for GTGs. It also demonstrates that strategy 1 is more considerate of the economic and low-carbon aspects than strategy 3.

The optimization results for DSO, LA, and EVA are discussed below.

1) Optimization results for DSO

The optimization results in Fig. 9 illustrate the complete accommodation of wind power generation by the test network under all three scheduling strategies. To address the uncertainty of wind power output, V2G service of EV fleets is utilized during periods of low wind power from 23:00 to 24:00 and during periods of peak load from 11:00 to 13:00 and 19:00 to 22:00. The scheduled EV discharging aids in compensating for the insufficient wind power, achieving a supply-demand balance and reducing the power demand for purchasing from transmission systems, thereby lowering overall carbon emissions. The charging behavior of EVA concentrates during the early morning periods from 01:00 to 07:00, reducing peak-to-valley differences and promoting low-carbon emission characteristics of EVs. This collaborative operation improves the low-carbon performance of all involved agents.

2) Optimization results for LA

The load-shifting results of LA under scheduling strategies 1-3 are shown in Fig. 10. It is observed that LA, driven by TOU electricity prices, exhibits a "peak-shaving and valley-filling" phenomenon in its load behavior. As electricity prices are higher during peak periods, i.e., 10:00 - 15:00 and 19:00 - 22:00, flexible consumers are incentivized to shift their power demand from peak hours to off-peak hours, i.e., 07:00 - 09:00, 16:00 - 18:00, and 23:00 - 06:00 on the next day, when electricity prices are lower. This leads to a modified load demand profile with a reduced difference between peak and valley loads, thereby decreasing in the required peak generation capacity. The load-shifting capability of LA is directly linked to the aggregated load power. Furthermore, consumers also reduce their electricity costs through participating in demand response.

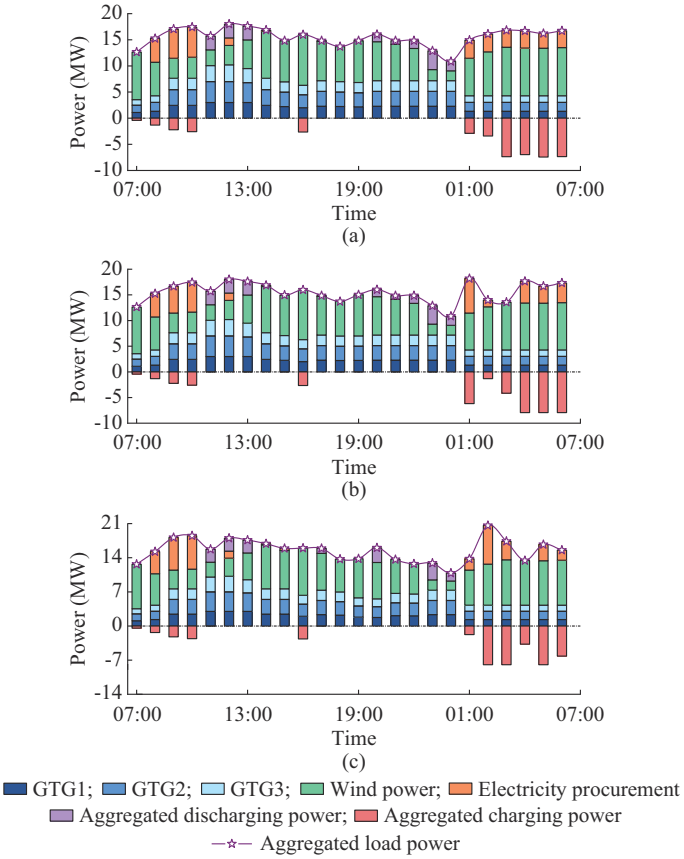

Fig. 9. Optimization results for DSO. (a) Strategy 1. (b) Strategy 2. (c) Strategy 3.

3) Optimization results for EVA

The optimization results for EVA under strategy 1 are shown in Fig. 11. It is observed that the charging power of aggregated EVs converges after 6 iterations. Initially, it fluctuates in the first few iterations before reaching stability, which is attributed to EVA pursuing the lowest cost in the initial iteration. With relatively low electricity prices during the specified period, EVs tend to charge centrally, rapidly increasing the charging power. The intermediate power fluctuations arise from the multi-agent bargaining, with a dynamic balance achieved.

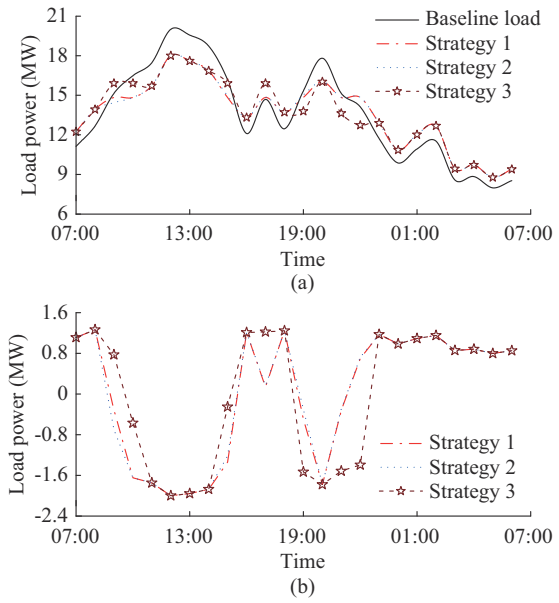

Fig. 10. Load-shifting results of LA under strategies 1-3. (a) Load power after demand response. (b) Transferrable load power.

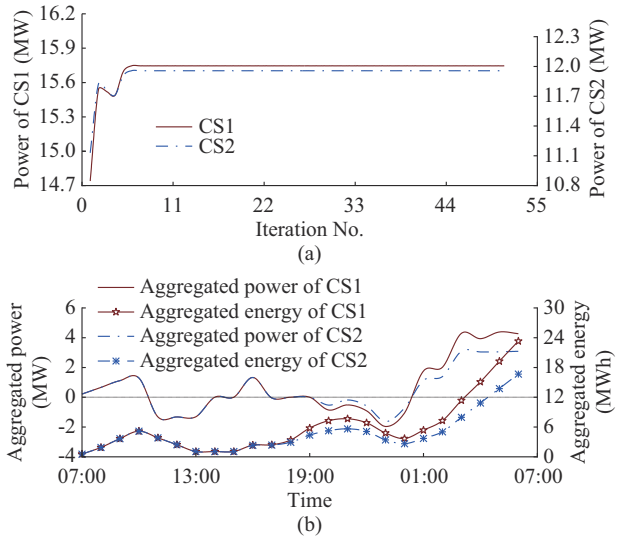

Fig. 11. Optimization results for EVA under scheduling strategy 1. (a) Charging power of aggregated EVs connected with CS1 and CS2 under different iterations. (b) Aggregated power and energy of CS1 and CS2 varying with time.

As shown in Fig. 11, after implementing strategy 1, the aggregated power and energy profiles exhibit fluctuating characteristics. This is because EV fleets dynamically switch between charging and V2G operation modes, according to the charging scheduling of EVA. For instance, during 07:00-10:00, the aggregated power gradually increases with the increasing aggregated energy, indicating an increase in the number of EVs being charged.

However, during 19:00 - 21:00, an opposite trend is observed between the aggregated power and energy curves. This is because EVs of nighttime charging start to charge during that period, leading to an increase in the aggregated energy. However, due to the peak power demand and high electricity prices, flexible EVs enter into V2G mode, decreasing the aggregated power.

4) Carbon emissions under strategy 1

From the perspective of DSO, its carbon emissions primarily stem from the equivalent carbon emission due to power procurement from transmission systems and the carbon emission from GTGs, as shown in Fig. 12. It is observed that strategy 1 exhibits a total carbon emission level similar to that of strategy 2. Compared with strategy 3, strategy 1 requires less power procurement and reduced power demand from GTGs, enhancing carbon reduction performance. The negative value in Fig. 12(b) indicates that the carbon emissions from GTGs are lower than the initially allocated carbon quota. In such a scenario, there is an excess of freely allocated carbon quota, which can be sold in the carbon trading market to generate profit. Consequently, the low-carbon units in the system are expected to have a higher power output, leading to increased revenue and enhanced low-carbon system performance.

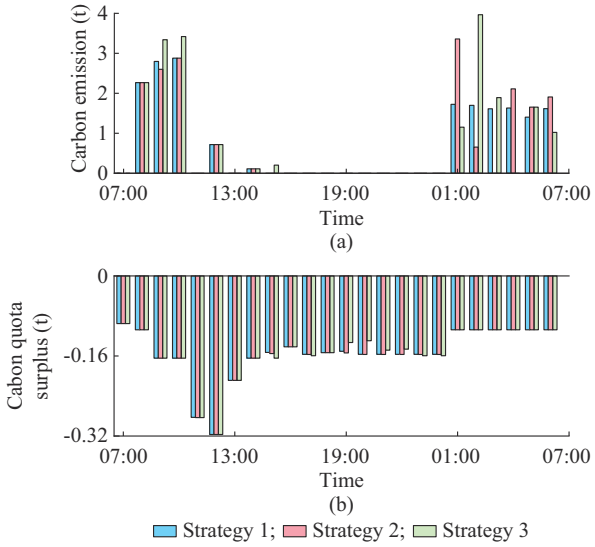

Fig. 12. Optimization results of carbon emissions. (a) Carbon emission due to power procurement. (b) Carbon emission from GTGs.

VII. Conclusion

The advancement of V2G technologies enables EVs to operate as battery storage units for grid interaction, representing an inevitable trend of the future smart grid. This paper establishes a source − load − storage cooperative low-carbon scheduling strategy considering V2G aggregators. It utilizes a Minkowski-sum based aggregation method to evaluate the scheduling potential of EV fleets while preserving their charging requirements. Subsequently, a Nash bargaining based cooperative scheduling model is proposed for DSO, EVA, and LA with integrated electricity and carbon trading. The model is then solved using an ADMM algorithm in a distributed manner. To accommodate uncertain EV charging patterns, the aggregation and co-scheduling strategies are implemented using a rolling-horizon control framework, where the control objectives and their scheduling horizon are dynamically updated. The proposed source−load−storage cooperative low-carbon scheduling strategy promotes coordinated low-carbon development in the power and transportation sec-

tors while preserving the information privacy of multiple agents.

Theoretical and arithmetic analyses illustrate the advantages of the proposed source−load−storage cooperative low-carbon scheduling strategy.

1) A rolling-horizon control framework is proposed to address uncertainty. Incorporating the rolling-horizon control framework allows the cooperative scheduling strategy to be executed in real time.

2) A Minkowski-sum based aggregation method is implemented to avoid the excessive variables and constraints being added during the direct sum of individual power flexibility models. It effectively reduces variable dimension and computational complexity while adhering to the charging/discharging constraints of individual EVs.

3) A Nash bargaining based cooperative scheduling model for DSO, EVA, and LA is proposed to pursue low-carbon economic co-scheduling. The model is solved using the ADMM algorithm in a distributed manner to preserve the privacy between agents.

REFERENCES

[1] IEA. (2022, May). Global EV Outlook 2022. [Online]. Available: https://www.iea.org/reports/global-ev-outlook-2022

[2] W. Dai, C. Wang, H. H. Goh *et al*., "Hosting capacity evaluation method for power distribution networks integrated with electric vehicles," *Journal of Modern Power Systems and Clean Energy*, vol. 11, no. 5, pp. 1564-1575, Sept. 2023.

[3] X. Shi, Y. Xu, Q. Guo *et al*., "Optimal dispatch based on aggregated operation region of EV considering spatio-temporal distribution," *IEEE Transactions on Sustainable Energy*, vol. 13, no. 2, pp. 715-731, Apr. 2022.

[4] G. Zhang, B. Xu, H. Liu *et al*., "Wind power prediction based on variational mode decomposition and feature selection," *Journal of Modern Power Systems and Clean Energy*, vol. 9, no. 6, pp. 1520-1529, Nov. 2021.

[5] W. Liao, S. Wang, B. Bak-Jensen *et al*., "Ultra-short-term interval prediction of wind power based on graph neural network and improved bootstrap technique," *Journal of Modern Power Systems and Clean Energy*, vol. 11, no. 4, pp. 1100-1114, Jul. 2023.

[6] X. Luo, D. Zhang, and X. Zhu, "Deep learning based forecasting of photovoltaic power generation by incorporating domain knowledge," *Energy*, vol. 225, p. 120240, Jun. 2021.

[7] Z. Jia, J. Li, X.-P. Zhang *et al*., "Review on optimization of forecasting and coordination strategies for electric vehicle charging," *Journal of Modern Power Systems and Clean Energy*, vol. 11, no. 2, pp. 389-400, Mar. 2023.

[8] C. Wu, S. Jiang, S. Gao *et al*., "Charging demand forecasting of electric vehicles considering uncertainties in a microgrid," *Energy*, vol. 247, p. 123475, May 2022.

[9] Q. Yan, H. Lin, J. Li *et al*., "Many-objective charging optimization for electric vehicles considering demand response and multi-uncertainties based on Markov chain and information gap decision theory," *Sustainable Cities and Society*, vol. 78, p. 103652, Mar. 2022.

[10] Y. An, Y. Gao, N. Wu *et al*., "Optimal scheduling of electric vehicle charging operations considering real-time traffic condition and travel distance," *Expert Systems with Applications*, vol. 213, p. 118941, Mar. 2023.

[11] M. Sedighizadeh, A. Mohammadpour, and S. M. M. Alavi, "A daytime optimal stochastic energy management for EV commercial parking lots by using approximate dynamic programming and hybrid big Bang big crunch algorithm," *Sustainable Cities and Society*, vol. 45, pp. 486-498, Feb. 2019.

[12] H. Yang, S. Zhang, J. Qiu *et al*., "CVaR-constrained optimal bidding of electric vehicle aggregators in day-ahead and real-time markets," *IEEE Transactions on Industrial Informatics*, vol. 13, no. 5, pp. 2555-2565, Oct. 2017.

[13] M. Firouzi, M. S. Nazar, M. Shafie-khah *et al*., "Integrated framework for modeling the interactions of plug-in hybrid electric vehicles aggregators, parking lots and distributed generation facilities in electricity markets," *Applied Energy*, vol. 334, p. 120703, Mar. 2023.

[14] S. A. Amamra and J. Marco, "Vehicle-to-grid aggregator to support power grid and reduce electric vehicle charging cost," *IEEE Access*, vol. 7, pp. 178528-178538, Oct. 2019.

[15] H. Lin, Y. Zhou, Y. Li *et al*., "Aggregator pricing and electric vehicles charging strategy based on a two-layer deep learning model," *Electric Power Systems Research*, vol. 227, p. 109971, Feb. 2024.

[16] P. Duan, B. Zhao, X. Zhang *et al*., "A day-ahead optimal operation strategy for integrated energy systems in multi-public buildings based on cooperative game," *Energy*, vol. 275, p. 127395, Jul. 2023.

[17] Y. Wang, X. Wang, C. Shao *et al*., "Distributed energy trading for an integrated energy system and electric vehicle charging stations: a Nash bargaining game approach," *Renewable Energy*, vol. 155, pp. 513-530, Aug. 2020.

[18] W. Wei, F. Liu, and S. Mei, "Charging strategies of EV aggregator under renewable generation and congestion: a normalized Nash equilibrium approach," *IEEE Transactions on Smart Grid*, vol. 7, no. 3, pp. 1630-1641, May 2016.

[19] S. Shojaabadi, V. Talavat, and S. Galvani, "A game theory-based price bidding strategy for electric vehicle aggregators in the presence of wind power producers," *Renewable Energy*, vol. 193, pp. 407-417, Jun. 2022.

[20] W. Wu, J. Zhu, Y. Liu *et al*., "A coordinated model for multiple electric vehicle aggregators to grid considering imbalanced liability trading," *IEEE Transactions on Smart Grid*, vol. 15, no. 2, pp. 1876-1890, Jul. 2023.

[21] P. Salyani, M. Abapour, and K. Zare, "Stackelberg based optimal planning of DGs and electric vehicle parking lot by implementing demand response program," *Sustainable Cities and Society*, vol. 51, p. 101743, Nov. 2019.

[22] H. Lin, J. Dang, H. Zheng *et al*., "Two-stage electric vehicle charging optimization model considering dynamic virtual price-based demand response and a hierarchical non-cooperative game," *Sustainable Cities and Society*, vol. 97, p. 104715, Oct. 2023.

[23] S. Abedi and S. Kwon, "Rolling-horizon optimization integrated with recurrent neural network-driven forecasting for residential battery energy storage operations," *International Journal of Electrical Power & Energy Systems*, vol. 145, p. 108589, Feb. 2023.

[24] A. Radaideh, A. Al-Quraan, H. Al-Masri *et al*., "Rolling horizon control architecture for distributed agents of thermostatically controlled loads enabling long-term grid-level ancillary services," *International Journal of Electrical Power & Energy Systems*, vol. 127, p. 106630, May 2021.

[25] Z. Yi, Y. Xu, W. Gu *et al*., "A multi-time-scale economic scheduling strategy for virtual power plant based on deferrable loads aggregation and disaggregation," *IEEE Transactions on Sustainable Energy*, vol. 11, no. 3, pp. 1332-1346, Jul. 2020.

[26] S. Barot and J. A. Taylor, "A concise, approximate representation of a collection of loads described by polytopes," *International Journal of Electrical Power & Energy Systems*, vol. 84, pp. 55-63, Jan. 2017.

[27] M. A. Ravindran, K. Nallathambi, P. Vishnuram *et al*., "A novel technological review on fast charging infrastructure for electrical vehicles: challenges, solutions, and future research directions," *Alexandria Engineering Journal*, vol. 82, pp. 260-290, Nov. 2023.

[28] A. G. Givisiez, K. Petrou, and L. F. Ochoa, "A review on TSO-DSO coordination models and solution techniques," *Electric Power Systems Research*, vol. 189, p. 106659, Dec. 2020.

[29] S. Li, L. Zhang, L. Nie *et al*., "Trading strategy and benefit optimization of load aggregators in integrated energy systems considering integrated demand response: a hierarchical Stackelberg game," *Energy*, vol. 249, p. 123678, Jun. 2022.

[30] F. Wei, Z. Jing, P. Wu *et al*., "A Stackelberg game approach for multiple energies trading in integrated energy systems," *Applied Energy*, vol. 200, pp. 315-329, Aug. 2017.

[31] J. Ding, C. Gao, M. Song *et al*., "Optimal operation of multi-agent electricity-heat-hydrogen sharing in integrated energy system based on Nash bargaining," *International Journal of Electrical Power & Energy Systems*, vol. 148, p. 108930, Jun. 2023.

[32] W. Zhong, S. Xie, K. Xie *et al*., "Cooperative P2P energy trading in active distribution networks: an MILP-based Nash bargaining solution," *IEEE Transactions on Smart Grid*, vol. 12, no. 2, pp. 1264-1276, Mar. 2021.

[33] Z. Zhang and K. S. Fedorovich, "Optimal operation of multi-integrated energy system based on multi-level Nash multi-stage robust," *Applied Energy*, vol. 358, p. 122557, Mar. 2024.

[34] S. Zeng, A. Kody, Y. Kim *et al*., "A reinforcement learning approach

to parameter selection for distributed optimal power flow," *Electric Power Systems Research*, vol. 212, p. 108546, Nov. 2022.
[35] X. Xie, J. Wu, G. Liu *et al.* (2019, May). Differentiable linearized ADMM. [Online]. Available: https://arxiv.org/abs/1905.06179
[36] T. Adefarati and R. C. Bansal, "Reliability assessment of distribution system with the integration of renewable distributed generation," *Applied Energy*, vol. 185, pp. 158-171, Jan. 2017.
[37] X. P. Zhan, J. Yang, S. N. Han *et al*., "Two-stage market bidding strategy of charging station considering schedulable potential capacity of electric vehicle," *Automation of Electric Power Systems*, vol. 45, pp. 86-96, Jan. 2021.
[38] S. Simkhada, M. Niraula, P. R. Ojha *et al*., "Time of use electricity pricing in power system planning and operation: case study of Nepalese power system," *Energy Reports*, vol. 8, pp. 825-831, Apr. 2022.
[39] D. Zeng, Y. Dong, H. Cao *et al*., "Are the electric vehicles more sustainable than the conventional ones? Influences of the assumptions and modeling approaches in the case of typical cars in China," *Resources, Conservation and Recycling*, vol. 167, p. 105210, Apr. 2021.
[40] Y. Wang, J. Qiu, Y. Tao *et al*., "Low-carbon oriented optimal energy dispatch in coupled natural gas and electricity systems," *Applied Energy*, vol. 280, p. 115948, Dec. 2020.
[41] Y. Huang, Y. Wang, and N. Liu, "Low-carbon economic dispatch and energy sharing method of multiple integrated energy systems from the perspective of system of systems," *Energy*, vol. 244, p. 122717, Apr. 2022.

Xiao Xu received his M. Sc. and Ph. D. degrees in the sustainable energy systems from University of Edinburgh, Edinburgh, UK, in 2013 and 2018, respectively. He is currently working as a Lecturer at Nanjing University of Posts and Telecommunications, Nanjing, China. His research interests include smart grid, power quality and low-carbon technologies.

Ziwen Qiu received his B. S. degree in electrical engineering from Jinling Institute of Technology, Nanjing, China, in 2022. He is currently pursuing the M. Sc. degree in electrical engineering from Nanjing University of Posts and Telecommunications, Nanjing, China. His research interest is smart grid.

Teng Zhang received his B. S. degree in electrical engineering from Southeast University Cheng Xian College, Nanjing, China, in 2022. He is currently pursuing the M. Sc. degree in electrical engineering from Nanjing University of Posts and Telecommunications, Nanjing, China. His research interest is power grid protection.

Hui Gao received his Ph.D. degree in the institute of electrical and mechanical from Nanjing University of Aeronautics and Astronautics, Nanjing, China, in 2011. He is working as a Professor in Nanjing University of Posts and Telecommunications, Nanjing, China. His research interests include electric vehicle and smart grid.